Modal Decomposition of Output Field for Holographic Mode Field Generation in a Multimode Fiber Channel

Angela Amphawan, Dominic O'Brien

Abstract—**Recent adaptive holographic equalization experiments in multimode fiber demonstrate the advantage of the rapid reconfiguration speed of the spatial light modulator in mitigating modal dispersion, the principal source of bandwidth limitation in MMF. Despite the suppression of a large number of modes, power modal coupling still manifests within the channel. In this paper, a noninterferometric modal decomposition technique was adapted for quantifying the amount of power modal coupling between the modes, for a holographic equalization experiment with *a priori* modal electric field input. The derivation of the objective function, simulation of binarized holograms and experimental work on intensity measurements at the MMF output are presented.**

***Index Terms*— noninterferometric modal decomposition, modal dispersion, power modal coupling, multimode fiber, spatial light modulator**

I. Introduction

Recent adaptive holographic equalization experiments in multimode fiber (MMF) demonstrate the advantage of the rapid reconfiguration speed of the spatial light modulator (SLM) in mitigating modal dispersion, the principal source of bandwidth limitation in MMF [2-4]. Two types of adaptive holographic equalization techniques are prevalent. In the first category, a random estimate at the onset of the optimization process was applied [2-4], while in others, an *a priori* modal electric field input was provided at the onset of the optimization [5]. The advantage of the provision of *a priori* input is the reduction in the number of iterations to achieve the optimum channel impulse response or bandwidth [5].

In the adaptive holographic equalization experiment with *a priori* input in [5], a good approximation to the theoretical modal electric field was generated for any desired lower-ordered mode and subsequently optimized successfully to achieve an increase in the channel bandwidth. Nevertheless inevitably, the optical power from the selective launch at the MMF input is gradually redistributed among the propagating modes within the MMF. This is caused by inherent perturbations in the symmetry of the optical fiber and manifests as power modal coupling [6]. In order to quantify the power modal coupling between the modes, a noninterferometric modal decomposition technique was used to acquire the distribution of the output electric field as a sum of the electric fields of individual modes in the MMF. This paper describes the derivation and steps for implementing the noninterferometric modal decomposition of the output electric field from the *a priori* adaptive holographic equalization experiment in [5].

The remainder of the paper is structured as follows. A basic outline of the adaptive holographic equalization experiment in is given in Section I. This is followed by the derivation of the error function for optimizing the power coupling coefficients in Section II. Section III outlines the steps for the simulation of binarized holograms for generating the required polarizations of the modal field. Finally, Section IV reports on the experimental work on intensity measurements at the at the MMF output.

Manuscript received [March 1, 2009]. The authors are at the Department of Engineering Science, University of Oxford, Oxford, UK and may be contacted at a.amphawan@seh.oxon.org.

II. Holographic Selective Mode Excitation Experiment

The holographic selective mode excitation technique for a MMF channel in [5] was realized using transmissive binary amplitude SLM and three lenses, as shown in Fig. 2. The lenses used were achromatic doublets of f_1=300mm (*L1*) and f_2=100mm (*L2*); and a collimator with an aspheric lens of f_3=11mm (*L3*). A 632.8nm Helium Neon laser was used. A visible laser was chosen for ease of alignment of optics and to easily view the generated modal field at various points along the system. A 128 x 128 pixel SLM was used to display the binarized modal electric field. The MMF used was a 1km-long graded-index Thorlabs GIF625, with a = 1.81.

The inherent modal electric field for the MMF for a perfect infinite parabolic MMF was generated experimentally. A preprogrammed binarized hologram of the desired mode was displayed on the SLM. A collimated beam from the laser was expanded 20 times and directed through the transmissive SLM. The binarized electric field on the SLM was then Fourier transformed by *L1*. The first diffraction order at the back Fourier plane of *L1* was then isolated. Following this, the *L2-L3* pair then scaled down the first diffraction order to the inherent size of the modal electric field of the MMF. The generated modal electric field was then adaptively optimized to maximize the channel bandwidth.

978-1-4244-7187-4/10/$26.00

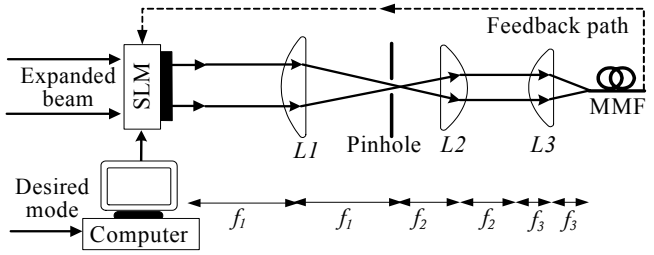

L1: first lens *L2*: second lens *L3*: third lens
f_1: focal length of *L1* f_2: focal length of *L2* f_3: focal length of *L3*

Fig. 2 Experimental setup

III. Derivation of Error Function for Optimization of Power Coupling Coefficients

The power coupling coefficient into LP_{lm} at the channel output is expressed as:

$$c_{lm} = \frac{\left| \iint_{A_{core}} \mathbf{E}_{out}(x,y)\, \mathbf{e}_{lm}^{*}(x,y)\, dx\, dy \right|^2}{\iint_{A_{core}} \left|\mathbf{E}_{out}(x,y)\right|^2 dx dy \iint_{A_{core}} \left|\mathbf{e}_{lm}(x,y)\right|^2 dx\, dy} \quad (1)$$

where $\boldsymbol{E_{out}}$ is the electric field at the output and $\boldsymbol{e_{lm}}$ is the transverse electric field for LP_{lm} mode of an infinite parabolic index of a weakly guiding graded-index MMF. The main advantage of the noninterferometric modal decomposition in [7] in calculating the power coupling coefficients, c_{lm} for the adaptive holographic equalization channel with *a priori* input is the relatively lower computational requirement for acquiring the distribution of c_{lm}, compared to directly calculating c_{lm} from Eq. (1). To use Eq. (1) , images of the electric fields of both the output from the MMF and the inherent LP_{lm} modes are required. The electric fields are dependent on the *x* and *y* coordinates. Also, the electric fields contain both amplitude and phase. Thus, a 4-dimensional variable is required for representing the electric fields for calculating c_{lm}. This requires a large number of pixels at hand for processing c_{lm} for each mode present in the output field. Also, in order to obtain the complete modal distribution of the output field, c_{lm} for all the modes present in the output field need to be computed individually. This is computationally intensive. On the other hand, in the noninterferometric modal decomposition [7], tensors are used to eliminate iterative usage of Eq. (1). Also, the only dependent variables are the complex c_{lm},, which are two-dimensional, as opposed to the two four-dimensional electric field images required in Eq. (1). Secondly, in order to calculate Eq. (1), the phase of output field is required. This is typically measured using an interferometer, which requires additional experimental apparatus, extra sensitivity and more complicated procedures. To eliminate the requirement for interferometry to retrieve the phase of the output field, the noninterferometric modal decomposition [7] is an elegant alternative. Also, although noninterferometric phase retrieval algorithms such as the Gerchberg-Saxton algorithm [8] and others [9-11] may be used, the solution of the modal decomposition may not be unique, as is the case with [7]. Thus, overall, the noninterferometric technique in [7] is more straightforward and efficient compared to using Eq. (1) for retrieving c_{lm}. Due to these advantages, the approach in [7] was taken for the noninterferometric modal decomposition of the output field from the adaptive holographic equalization experiment in [5].

TABLE I
Modal Transverse Fields of a Weakly-Guiding Infinite Parabolic Multimode Fiber [1]

Degenerate forms for $\mathbf{e}_{lm}$	
$\{\hat{\mathbf{x}}\cos l\phi - \hat{\mathbf{y}}\sin l\phi\} F_l$	$\{\hat{\mathbf{x}}\sin l\phi + \hat{\mathbf{y}}\cos l\phi\} F_l$
$\{\hat{\mathbf{x}}\cos l\phi + \hat{\mathbf{y}}\sin l\phi\} F_l$	$\{\hat{\mathbf{x}}\sin l\phi - \hat{\mathbf{y}}\cos l\phi\} F_l$

where $\hat{\mathbf{x}}$ and $\hat{\mathbf{y}}$ are unit vectors parallel to the *x*- and *y*-axes respectively and orthogonal to the MMF cross-section. F_{lm} is the radial dependence of the electric field of the LP_{lm} mode, given in Eq. (3).

The objective is to reconstruct the measured intensity at the MMF output in terms of e_{lm} of a weakly-guiding infinite parabolic graded-index MMF, such that the difference between the reconstructed estimate of the measured intensity and the actual measured intensity is minimized.

Modes in a weakly-guiding MMF are commonly known as linearly polarized modes or LP_{lm} modes, where l = 0, 1, 2.. is the azimuthal mode number and m = 1, 2,... is the radial mode number. The transverse electric field for the LP_{lm} mode of the weakly guiding graded-index MMF may be expressed as:

$$e_{lm}(x,y) = e_{x_{lm}}(x,y)\,\hat{\mathbf{x}} + e_{y_{lm}}(x,y)\hat{\mathbf{y}} \quad (2)$$

where $e_{x_{lm}}$ and $e_{y_{lm}}$ are the *x* and *y* components of the transverse electric field for the LP_{lm} mode. The degenerate forms for e_{lm} for the LP_{lm} mode in a weakly-guiding infinite parabolic MMF, $\boldsymbol{e_{lm}}$ are given in Table 1 [1]. The radial dependence of the transverse electric field is given by:

$$F_{lm} = R^{l} L_{m-1}^{(l)}(VR^2)\exp(-0.5VR^2). \quad (3)$$

where the function $L_{m-1}^{(l)}$ is the generalized Laguerre polynomial, R is the normalized core radius and V is the normalized frequency. The total electric field is the sum of the transverse electric fields for all LP_{lm} modes:

$$\vec{E}(x,y) = \sum_{lm} c_{lm} e_{lm}(x,y) \quad (4)$$

where c_{lm} is the complex output power coupling coefficient of the transverse electric field for the LP_{lm} mode in Eq. (1). The complex c_{lm} may be expressed as:

$$c_{lm} = |c_{lm}| \exp(ik_{lm}) \quad (5)$$

where $|c_{lm}|$ is the absolute value of the output power coupling coefficient for the LP_{lm} mode and k_{lm} is the phase of the output power coupling coefficient for the LP_{lm} mode.

In order to obtain a unique solution for the reconstructed field, four output measurements are taken. One measurement is taken for each of the two polarizations of the MMF. For each polarization, the measurement is taken in the near-field and also the far-field. The difference between the reconstructed estimate of the measured intensity and the actual measured intensity is described in terms of the error function, expressed as below, following [7]:

$$\Delta_{a,b} = \int_{core} \left\{ I_r^{a,b}(r) - I_o^{a,b}(r) \right\}^2 dA \tag{6}$$

where I_o is the measured output intensity, I_r is the reconstructed estimate of the measured intensity. a defines the plane of measurement, where a=1 is the near field plane and a=2 is the far field plane. b defines the two orthogonal polarizations of transverse electric field of the weakly guiding MMF, given by:

$$b = \begin{cases} 1, & \vec{E} = F_{lm} \cos(l\phi) \\ 2, & \vec{E} = F_{lm} \sin(l\phi) \end{cases} \tag{7}$$

where l is the azimuthal mode number, m is the radial mode number and F_{lm} is the radial dependence of the electric field of the LP_{lm} mode in Eq. (3). The overall error function is the sum of the error functions for the near-field, far-field and two orthogonal polarizations, given as, adapted from [7]:

$$\Delta = \sum_{a,b} \Delta_{a,b} \tag{8}$$

Instead of using both the magnetic and electric fields as in [7], here, only the electric field is used. Also, the order of the tensors in [7] has been reduced to simplify computation.

The reconstructed estimate of the measured intensity, I_r can be rewritten in terms of output power coupling coefficients of the transverse electric fields for the LP_{lm} modes,

$$I_r(x,y) = \frac{1}{N} \sum_{l_1 m_1 l_2 m_2} c_{l_1 m_1} c^*_{l_2 m_2} \cdot \left[e_{x_{l_1 m_1}}(x,y)\,\hat{\mathbf{x}}\; e_{x_{l_2 m_2}}(x,y)\,\hat{\mathbf{x}} \;.... + e_{y_{l_1 m_1}}(x,y)\, e_{y_{l_2 m_2}}(x,y)\hat{\mathbf{y}} \right] \tag{9}$$

where N is power normalization factor. Substituting (9) into (6), the error function may be written in terms of the output power coupling coefficients:

$$\Delta_{a,b} = \frac{1}{N^2} \cdot \sum_{l_1 m_1 l_2 m_2 l_3 m_3 l_4 m_4} c_{l_1 m_1} c^*_{l_2 m_2} c_{l_3 m_3} c^*_{l_4 m_4} \Lambda_{l_1 m_1 l_2 m_2 l_3 m_3 l_4 m_4} - \frac{2}{N} \sum_{l_1 m_1 l_2 m_2} c_{l_1 m_1} c^*_{l_2 m_2} \Gamma_{l_1 m_1 l_2 m_2} + P \tag{10}$$

where $c_{l_n m_n}$ is the power coupling coefficient for the LP_{lm} mode of a weakly-guiding infinite parabolic MMF at the MMF output, where the subscripts l_n and m_n are the n-th index for the azimuthal and radial mode numbers respectively, and the measured output power is given by:

$$P(x,y) = \int_{core} I_{me}^2(x,y)\, dx\, dy. \tag{11}$$

The tensors in eq. (10) were derived using only the electric field, instead of both the magnetic and electric fields as in the derivation in [7]. Also, in our derivation, the order of the indices of tensor $\Lambda_{l_1 m_1 l_2 m_2 l_3 m_3 l_4 m_4}$ was reduced from 4 to 3, by implicitly summing repeated indices [12-14] as follows:

$$\Lambda_{l_1 m_1 l_2 m_2 l_3 m_3 l_4 m_4 2} c_{l_3 m_3} c^*_{l_4 m_4} = \Lambda_{l_1 m_1 l_2 m_2 l_3 m_3} \tag{12}$$

Thus, the derived tensors may be expressed as:

$$\Gamma^{a,b}_{l_1 m_1 l_2 m_2} = \int_{core} I^{a,b}_{me} \left[e_{x_{l_1 m_1}}(x,y)\, e_{x_{l_2 m_2}}(x,y) + e_{y_{l_1 m_1}}(x,y)\, e_{y_{l_2 m_2}}(x,y) \right] dA \tag{13}$$

$$\Lambda_{l_1 m_1 l_2 m_2 l_3 m_3 l_4 m_4} = \int_{A\,core} \left[e_{x_{l_1 m_1}}(x,y)\, e_{x_{l_2 m_2}}(x,y) + e_{y_{l_1 m_1}}(x,y)\, e_{y_{l_2 m_2}}(x,y) \right] \left[e_{x_{l_3 m_3}}(x,y)\, e_{x_{l_4 m_4}}(x,y) + e_{y_{l_3 m_3}}(x,y)\, e_{y_{l_4 m_4}}(x,y) \right] dA \tag{14}$$

where $e_{x\,l_n m_n} = F_{lm} \cos(l\phi)$, $e_{y\,l_n m_n} = F_{lm} \sin(l\phi)$ and the subscripts l_n and m_n are the n-th index for the azimuthal and radial mode numbers respectively.

IV. Simulation of Holograms for x-Polarized and y-Polarized Electric Fields

The noninterferometric modal decomposition described in Section III requires two orthogonal polarizations of the input electric field for each excited mode, in order to obtain two corresponding orthogonal polarizations of the electric field at the output. Accordingly, binarized holograms for the two orthogonal polarizations were simulated for each mode to be excited, following the approach in [15]. Typical binarized holograms of two orthogonal polarizations for the desired mode are shown in Fig. 2.

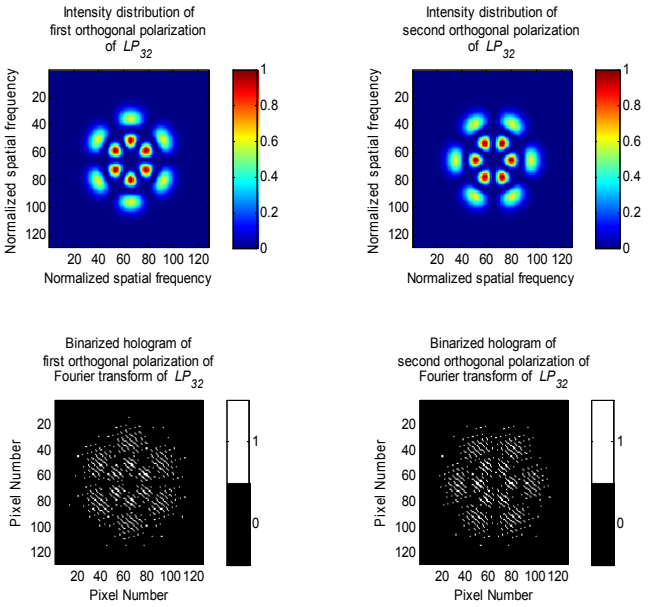

Fig. 2 Binarized holograms for two orthogonal polarizations of the LP_{32} mode. *1* indicates intensity transmission and *0* indicates no intensity transmission

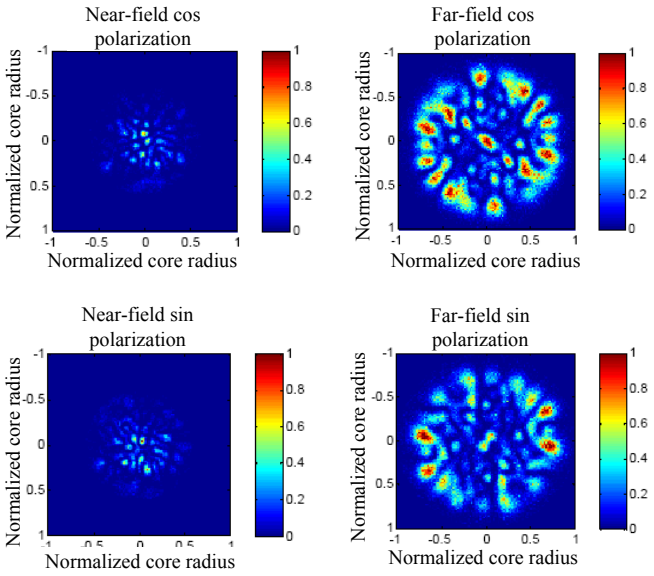

Fig. 4 A set of four measured output intensity distributions for noninterferometric modal decomposition of the modal generation and adaptive optimization of the L_{44} mode

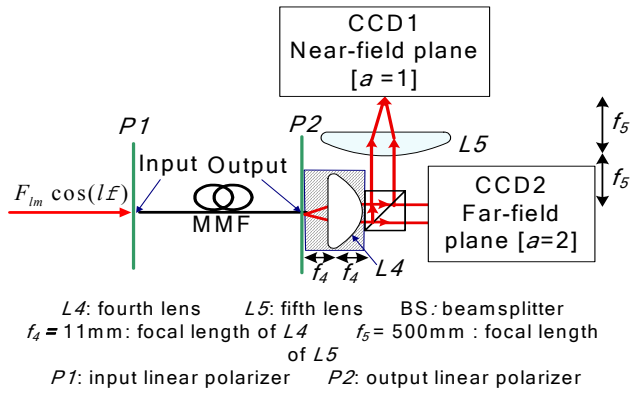

Fig. 3 Experimental setup and procedure for recording four output intensity distributions from MMF for noninterferometric modal decomposition for the F_{lm} *cos* (l∠) polarization

V. Experiment and Measurements of Output Intensity Distributions from Holographic Selective Mode Excitation Launch

The experimental setup and procedure for the measurement of the near-field and far-field intensities of the output is shown in Fig. 3. The near-field and far-field planes and the CCD cameras used for measuring each plane are indicated. The output endface of the MMF was connected to a fiber collimator containing an aspheric lens *L4* of focal length f_4=11mm. *L4* Fourier transforms the electric field in the plane of the output endface of the MMF. The resultant image is formed in the back focal plane of *L4* and captured by CCD2. This plane is known as the far-field plane of the MMF output.

Before recording the required intensity distributions, the input and output linear polarizers *P1* and *P2* were calibrated so as to obtain two sets of orthogonal electric fields, at the input and the output of the MMF. For the calibration of *P1,* the binarized hologram for the F_{lm} *cos* (l∠) polarization of the electric field for LP_{01} was displayed on the SLM. The angle of *P1* was rotated such that the intensity of the generated modal field was *maximum*. This angle, φ_{ci} was noted and was set on *P1* for all F_{lm} *cos* (l∠) polarization measurements. With the binarized hologram for the F_{lm} *cos* (l∠) polarization of the electric field of the LP_{01} mode still displayed on the SLM, the angle of *P1* was rotated such that the intensity of the generated modal field was *minimum*. This angle, φ_{si} was noted and was set on *P1* for all F_{lm} *sin* (l∠) polarization measurements. The same procedure was repeated for the calibration of P2, this time minimizing the received intensity distribution from the transmission of the *minimized* F_{lm} *cos* (l∠) polarization of the electric field of $LP_{01.}$

The position and orientation of the SLM and all optics after the calibration of *P1* and *P2* are preserved. The steps for recording the four sets of intensity distributions are described as follows: For setup for recording the intensity distributions for the F_{lm} *cos* (l∠) (b=1) is shown in Fig. 3. First, the binarized hologram for the F_{lm} *cos* (l∠) polarization of the electric field of the desired mode was transmitted by displaying the corresponding binarized hologram described in Section I was displayed on the SLM. *P1* was set to φ_{ci} and *P2* was set to φ_{co}. Then, the received output intensity distributions

were recorded by CCD2 in the far-field ($a=2$) and by CCD1 in the near-field ($a=1$). The same procedure is repeated for recording the F_{lm} *sin* ($l\phi$) polarization ($b=2$) intensity distributions of the electric field of the desired mode. However, this time, *P1* was set to φ_{si} and *P2* was set to φ_{so}. A typical set of the four measured output intensity distributions is shown in Fig. 4.

VI. Conclusion

A noninterferometric modal decomposition technique was used to quantify the amount of power modal coupling between the modes for an adaptive holographic equalization experiment with *a priori* modal electric field input in a MMF channel. The derivation of the objective function and tensors, simulation of binarized holograms and experimental work on intensity measurements at the MMF output have been presented.

References

[1] A. W. Snyder and J. D. Love, *Optical waveguide theory*. London: Chapman and Hall, 1983.

[2] E. Alon*, et al.*, "Equalization of modal dispersion in multimode fiber using spatial light modulators," in *GLOBECOM '04. IEEE Global Telecommunications Conference*, Dallas, TX, USA, 2004, pp. 1023- 1029.

[3] P. L. Neo*, et al.*, "Modal Control of a 50µm core diameter Multimode Fiber Using a Spatial Light Modulator," in *Optical Fiber Communication and the National Fiber Optic Engineers Conference, 2007. OFC/NFOEC 2007. Conference on*, 2007, pp. 1-3.

[4] E. Alon*, et al.*, "Equalization of Modal Dispersion in Multimode Fiber using Spatial Light Modulators," in *Proc. of IEEE Global Telecommun. Conf.*, Dallas, TX, 2004.

[5] A. Amphawan and D. O'Brien, "Holographic Mode Field Generation for a Multimode Fiber Channel," in *International Conference on Photonics 2010 (ICP2010)*, Langkawi, 2010.

[6] D. Marcuse, *Theory of dielectric optical waveguides. 2nd ed.* , 1991.

[7] O. Shapira, et al., "Complete modal decomposition for optical waveguides," Physical Review Letters, vol. 94, pp. 143902/1-4, 15 April 2005.

[8] R. W. Gerchberg and W. O. Saxton, "A practical algorithm for the determination of phase from image and diffraction plane pictures," Optik, vol. 35, pp. 237-46, 1972.

[9] R. W. Gerchberg, "A new approach to phase retrieval of a wave front," Journal of Modern Optics, vol. 49, pp. 1185-96, 15 June 2002.

[10] K. A. Nugent, et al., "Quantitative phase imaging using hard X-rays," Proceedings of the SPIE The International Society for Optical Engineering, vol. 3154, pp. 110-16, 1997.

[11] M. G. Raymer, et al., "Complex wave-field reconstruction by using phase-space tomography," in IQEC'94. International Quantum Electronics Conference. Anaheim, CA, USA. Opt. Soc. America. IEEE/Lasers & Electro Opt. Soc. American Phys/ Soc. U.S. Joint Council on Quantum Electron. Int. Council on Quantum Electron. Int Comm. Optics. Int. Union of Pure & Appl. Phys. 8 13 May 1994., 1994.

[12] G. T. Mase and G. E. Mase, Continuum mechanics for engineers, 2nd ed. / G. Thomas Mase, George E. Mase. ed. Boca Raton, Fla. ; London: CRC Press, 1999.

[13] G. B. Arfken and H. J. Weber, Mathematical methods for physicists, 5th ed. ed. San Diego, Calif. ; London: Harcourt Academic, 2001.

[14] R. Aris, Vectors, tensors, and the basic equations of fluid mechanics: Dover, 1989.

[15] M. A. A. Neil, et al., "A wavefront generator for complex pupil function synthesis and point spread function engineering," Journal of Microscopy, vol. 197, pp. 219-23, March 2000.